X-621-71-22
PREPRINT

NASA TM X- 65435

EXPERIMENTAL VERIFICATION OF THE THEORY ON WEAK TURBULENCE — INTERPRETATION OF SEQUENCE OF DIFFUSE PLASMA RESONANCE OBSERVED IN SPACE

HIROSHI OYA

JANUARY 1971

GODDARD SPACE FLIGHT CENTER
GREENBELT, MARYLAND

X-621-71-22

EXPERIMENTAL VERIFICATION OF THE THEORY ON WEAK TURBULENCE – INTERPRETATION OF SEQUENCE OF DIFFUSE PLASMA RESONANCE OBSERVED IN SPACE

Hiroshi OYA*

January 1971

*NAS-NRC Resident Research Associate

NASA Goddard Space Flight Center
Greenbelt, Maryland

ABSTRACT

An interpretation of the sequence of diffuse plasma resonances observed by space probes (Alouette 2 and ISIS-A satellites) is developed in terms of wave-particle nonlinear interaction in a weakly turbulent plasma including electostatic electron cyclotron harmonic wave instability. Observations and theory indicate that the center frequency f_{Dn} of the diffuse plasma resonance ($nf_H < f_{Dn} < (n+1)f_H$ and $f_{Dn} < f_T$) and the center frequency of the electrostatic wave resonance ($nf_H < f_{Dn} < (n+1)f_H$ and $f_T < f_{Qn}$) satisfy the condition of the wave particle nonlinear interaction with the $2f_H$ resonance according to the condition $2\pi \{2f_H - (f_{Qn+2} - f_{Dn})\} = \{\vec{k}(f_{Q\ n+2}) - \vec{k}(f_{Dn})\} \cdot \vec{v}$ where nf_H, f_T and $\vec{v}$ are the cyclotron harmonic frequency the upper hybrid frequency and thermal velocity of plasma, respectively. The weaker diffuse plasma resonance branch observed at f_{Dn1} (where $f_{Dn1} < f_{Dn}$) satisfies the condition $2\pi \{f_H - (f_{Qn+1} - f_{Dn1})\} = \{\vec{k}(f_{Qn+1}) - \vec{k}(f_{Dn})\} \cdot \vec{v}$. The longest time durations of the f_{Dn} resonance coincides with the most favorable condition for the electrostatic electron cyclotron harmonic wave instability which is obtained by solving the dispersion equation obtained for a linear approximation of kinetic equation for the warm magnetoactive plasma. The electrostatic field due to the transmiss. n of the intense RF pulse triggers plasma turbulence involving nonlinear wave-

wave interaction and temperature anisotropy which leads to the instability ; this instability supplies energy to the turbulence. The f_H and $2f_H$ wave produced in the nonlinear wave-wave interaction in the turbulence heat up the plasma to maintain the temperature anisotropy which lengthens the time over which the cyclotron harmonic wave instability conditions prevail ; this process can be thought of as a feed bach system. The results also indicate that the f_H, $2f_H$ and f_{Qn} wave are dependent on the f_{Dn} resonance generation.

I. Introduction

Prolonged responses to a transmitted RF pulse are observed in the experimental data obtained by the topside sounder satellites ; these responses have been called plasma resonances[1]. In Fig.1 a sample record obtained by the Alouette 2 satellite is shown in the conventional ionogram format[2]. The response to the transmitted RF pulse with 100μsec pulse width is recorded on the ordinate during the 33msec time interval following the transmitted pulse. The frequency of the receiver and the transmitter are swept simultaneously from 0.12 to 14.5MH_z and are displayed on the abscissa to form the so-called ionogram, i. e., automatic frequency scanning system for the diagnosis of the plasma using RF waves. The indicated plasma resonances are interpreted in the figure caption. Particular interest to the present discussion is the diffuse plasma resonance f_{D1} which was first identified by Nelms and Lockwood[3]. (they used the notation f_D for this resonance). They reported that the resonance occurs frequently near $1.5f_H$ and sometimes near $f_T/2$ or $f_N/2$, depending on the local plasma conditions, where f_H is the electron gyrofrequency, f_T is the upper hybrid resonance frequency and f_N is the plasma frequency. A more extensive investigation[4] has revealed that f_{D1} follows an expirical relationship with f_N/f_H and that there are additional diffuse type plasma resonances which together with the f_{D1} resonance, form a sequence of diffuse resonances observed at the frequencies f_{Dn} between f_H and $(n+1)f_H$ where n=1,2,3, and 4; and f_{D1} corresponds to the earliar f_D notation.

The purpose of the present paper is to offer an interpretation of this sequence of diffuse plasma resonances, and to show an experimental confirmation to a weak turbulence theory on wave particle nonlinear interaction which is summarized by Sagdeev[5]. There are two additional sequences of plasma resonances ; one if the famous sequence of cyclotron harmonic resonances[6] which occurs at nf_H and the other is the resonance sequence observed by Warren and Hagg[7] observed at the frequency f_{Qn} where $nf_H < f_{Qn} < (n+1)f_H$, for n=2, 3 and 4. The present work indicates that the f_{Dn} resonances are generated by a nonlinear wave-wave interaction, involving f_{Qn} and $2f_H$ or f_H, and the instability of the electrostatic electron cyclotron harmonic waves under a weak nonlinear interacion. The results also indicate that the previously given interpretations of f_H, $2f_H$[8, 9] and f_{Qn} resonances should be modified so as to include this wave-particle nonlinear interaction.

II. Observation of Sequence of Diffuse Plasma Resonance

II.1. Summary of Sequence Diffuse Plasma Resonance

The sequence of Diffuse plasma resonances observed at the frequencies[4] f_{Dn} will be reffered to simply as f_{Dn} in the remainder of this work. In Fig.2 these resonances, in addition to the resonances observed at f_N, f_T, nf_H and f_{Qn} are presented in a plot of normalized resonant frequency (with respect to f_H) vs. the plasma parameter f_N/f_H. This diagram represents a convenient summary of previous observations of the resonances that will be

of interest in the present discussion. Important information concerning the resonant phenomena can also be obtained by measuring the time duration of the resonant signal. In Fig.3, the time durations have been plotted as scaled from 370 ionograms which were randamly sampled from the f_{Dn} data source observed at Quito and Santiago telemetry stations[4]. The results are indicated versus the normalized resonance frequency f_{Dn}/f_H.

The main points of the above mentioned f_{Dn} and time duration measurement of the f_{Dn} resonances are summarized in the following 6 statements :

1. The f_{Dn} resonance have several groups corresponding to n values of 1 to 4 ; f_{Dn} corresponding to higher n values than 5 have not been definitly identified due to observational difficulties. The observed frequency ranges of the individual groups are clearly separated from one another.
2. Sometimes, the f_{Dn} resonances are accompanied by weaker resonances, which lead to additional branches separated from the main f_{Dn} branch on the f_{Dn}/f_H versus f_N/f_H diagram. Two weaker resonances, corresponding to a given n value are never observed simultaneously and the weaker resonances occur less frequently than the main branch resonances. There are two weaker resonance branches in the f_{D1} group, one on the high frequency side (here this is called f_{D11}) and the other on the low frequency side (here this is called f_{D12}) of the main branch . In the f_{D2} group, there is only one weaker reso-

nance branch that is on the high frequency side; this is called f_{D21} in the present work. The f_{D3} and f_{D4} resonances have, sometimes, weaker secondary resonance peaks but no significant statistical separation from the main branch is observed.

3. In the f_{D1} and f_{D2} groups, f_{Dn}/f_H increases monotonically with f_N/f_H with an indication of a dip near $f_N/f_H \simeq 3$ for f_{D1} and the suggestion of dip near $f_N/f_H \simeq 4$ for f_{D2}.
4. The time duration of f_{D1} is about 3 to 5 times longer in the frequency range $1.5 \lesssim f_{D1}/f_H \lesssim 1.63$ than in the other portion of the observed frequency range for f_{D1} ; similarly, the time duration of f_{D2} is 2 to 3 times longer in the frequency range $2.65 \lesssim f_{D2}/f_H \lesssim 2.82$ than in the other portion of the observed frequency range for f_{D2}. Such a sharp peaking of the time duration is not apparent for f_{D3} and f_{D4}.
5. The time duration of f_{Dn} gradually decreases with increasing n. The following maximum values have been observed : f_{D1} = 24msec, f_{D2} = 10.8msec, f_{D3} = 4msec and f_{D4} = 1.5msec.
6. The frequency f_{Dn} are related to the f_{Qn} resonance frequency in the following manner :

$$f_{D1} = f_{Q3} - 2f_H \qquad (1)$$

$$f_{D2} = f_{Q4} - 2f_H \qquad (2)$$

$$f_{D11} = f_{Q2} - f_H \qquad (3)$$

and $$f_{D21} = f_{Q3} - f_H \qquad (4)$$

The f_{Qn}(n=2,3 and 4) resonant frequencies coincide with f_T resonant frequency in the certain range of plasma parameter . In this case eqs.(3) and (4) are also satisfied by f_T which is actually same with f_{Qn}. Concerning the above 6 statements, Nos. 1,2 and 3 are summarized in more detail in a previous paper[4] while No.4 and No.5 present additional information reported here for the first time, and No.7 presents the results of a comparison of the f_{Dn} frequency information[4] with the f_{Qn} frequency information[7] .

II.2. f_{D1} and f_{Q3} in ISIS-A Satellite

The ISIS-A ionosphere topside sounder experiment includes the so called mixed mode experiment[10] in which the frequency of the receiver is swept from 0.1MH_z to 20MH_z. An example of this mixed mode experiment is shown in Fig.4. In this case no ionospheric echo exists but plasma resonances are observed at f_{D1}, $2f_H$, f_N, f_T and f_{Q3} even though the frequency of the exciting source is fixed at 0.82 MHz . In this mode of operation, the f_H resonance is much shorter in duration time than the other resonances observed ; and sometimes it becomes hard to recognize. Similarly the $3f_H$ resonance and the resonances at higher harmonics of nf_H are always much weaker than the $2f_H$ resonance and are sometimes hard to recognize.

The coexistence of the f_{D1}, $2f_H$ and f_{Q3} resonances in this mixed mode experiment is of fundamental importance in the present discussion. The center frequencies of the above resonances were

scaled on 19 ionograms from two randamly selected passes over the Ottawa telemetry station ; the results indicated that the average value for the quantity $(f_{Q3}-f_{D1})/f_H$ was found to be 1.96. Thus eq(1) in statement No.6 of Sect. II is also valid for this mixed mode experiment. These observations clearly suggest that the resonances observed at the frequencies f_{D1}, $2f_H$ and f_{Q3} are the result of a nonlinear process in the ionospheric plasma because the transmitter has no frequency component in its spectrum at these frequencies.

III. Trigger of Turbulence by Sounder Pulse

A generation of nonlinear process is suggested when the high power of the transmitted pulse is considered. The ISIS-A topside sounder transmits[10] a maximum power of 400 W during a time interval of 100 μsec. When the wave propagates with a velocity close to the electron thermal velocity (this is the case for the usual propagation of electrostatic electron cyclotron waves except for frequency ranges near cyclotron harmonic frequencies). The energy E excited by a dipole antenna with tip to tip length with group velocity v_g in a time interval T can cover a cylindrical volume $\pi v_g^2 \tau (2T-\tau)$ for $T > \tau$ where τ is the pulse width ; and here an uniform distribution of the energy in the cylindrical volume is assumed. The energy density is then expressed by $E\tau/\pi v_g^2 \tau (T-\tau)$ For L=73 m [10], $v_g = \sqrt{\kappa T_e/m}$ with edectron temperature T_e = 5000°K (K is Boltzmann and m is the electron mass) ; and for τ = 100 μsec the energy density is 2.30×10^{-6} erg/cm^3. This energy density is

two orders of magnitude larger than the electron thermal energy density of $6.9 \times 10^{-9}/cm^3$ corresponding to $T_e = 5000°K$ and $N_e = 10^4 cm^{-3}$ (these values are considered to give the maximum possible plasma energy density in the topside ionosphere) indicating the strong possibility of a nonlinear interaction.

The absorption rate of the transmitted plasma wave energy can be obtained from equation 53 of chapter 9 of Stix[11]. The absorption rates perpendicular and parallel to the earth's magnetic field vector $\vec{B}_0$ are found to be

$$R_\perp = \frac{\frac{1}{2} Ne\,(\vec{V}_\perp^* \cdot \vec{E}_\perp + \vec{V}_\perp \cdot \vec{E}_\perp^*)}{\frac{1}{2} \langle \vec{E}_\perp \cdot \vec{E}_\perp^* \rangle}$$

$$R_\parallel = \frac{\frac{1}{2} Ne\,(\vec{V}_\parallel^* \cdot \vec{E}_\parallel + \vec{V}_\parallel \cdot \vec{E}_\parallel^*)}{\frac{1}{2} \langle \vec{E}_\parallel \cdot \vec{E}_\parallel^* \rangle}$$

where N, e, $V_\parallel$, $V_\perp$, $E_\parallel$, and $E_\perp$ are electron density, electron charge, the electron average velocity parallel and perpendicular to $\vec{B}_0$, and the components of the plasma wave electric field vector parallel and perpendicular to B_0, respectively (* is used to denote the complex conjugate quantity). $V_\parallel$, $V_\perp$ are related to $E_\parallel$, $E_\perp$ through the movility tensor. Numerical calculations as presented in Fig.5, indicate that electrons are accelerated in the direction perpendicular to $\vec{B}_0$, i. e., $R_\perp > 0$ while they are deccelerated in the direction parallel to $\vec{B}_0$, i. e.. $R_\parallel < 0$, when

$q=f/f_H > 1.5$. The result values can obtain by multiplying $(q_N^2/2q)$ to the value which is read from the diagram. The quantity $R_\perp$ is about 10^{-2} in the frequency range around $1.6f_H$ it increases to the order of 10^{-1} as the frequency approaches $2f_H$ where the absorption is most efficient. The energy absorption rate for $q_N=2.0$ and $1.6 < q < 1.9$ is then in a range from about 6.0×10^{-3} to 2.6×10^{-1}. Thus the plasma energy is increased by approximately 2.0 to 86 times the unperterbed thermal energy level depending on the value of q.

The above linear calculations indicate that the transverse electrons temperature should be greater than the longitudinal temperature. Similar results is obtained for the Alouette 2 experiment since the power with the same order of magnitude (300 W as compared with 400 W for ISIS-A) is supplied. Thus, the trigger pulse produces a turbulent situation in the plasma ; the observations given in Sect.II are strictly experimental facts relating to this turbulence.

IV. Three-Wave Resonant Interaction and f_{Dn} Frequency

IV. 1. Weak Turbulent Approximation and Dispersion Relation

Kadomtsev[12] has considered a weak plasma turbulence in which only three waves have important roles for a nonlinear wave-wave interaction. The three wave can exist together only when dispersion relations $\vec{k}_1 = \vec{k}_1(f_1)$, $\vec{k}_2 = \vec{k}_2(f_2)$ and $\vec{k}_3 = \vec{k}_3(f_3)$

satisfy the following relations

$$f_3 = f_1 + f_2 \tag{7}$$

$$\vec{k}_3 = \vec{k}_1 + \vec{k}_2 \tag{8}$$

Kadomtsev called this nonlinear coupling a three wave decay process because the energy initially excited at one of the frequencies is shared with the waves at the other two frequencies. The theory was initially presented macroscopically and then expanded to include microscopic effects.

Sjölund[13] considered the three wave decay process in a magnetoactive plasma using the macroscopic hydrodynamic equation. Sagdeev and Galeev[14] investigated thermal particle motions in a magnetoactive plasma and their equation(III-39) indicates that the three wave decay process also plays an important role in the magnetoactive plasma. They called the process wave-wave resonant interaction. In all of the above work the assumption of weak turbulence is applied ; thus the dispersion relations of the individual waves are obtained by neglecting the nonlinear coupling term. In order to illustrate this procedure, let us consider the Kinetic wave equation for a thermal plasma as obtained by Kadomtsev (eq II 39), but modified so as to include an applied constant magnetic field, which is equivalent to a general treatment of Kennel and Engelmann[15], i.e.,

$$- i\left(\omega - \vec{k}\cdot\vec{V} - i\frac{e}{m}(\vec{V}\times\vec{B}_0)\cdot\frac{\partial}{\partial\vec{V}}\right) f_{\vec{k}\omega} = -\frac{e}{m}\cdot\vec{k}\,\frac{\partial f}{\partial\vec{v}}\,\varphi_{\vec{k}\omega}$$

$$- i\frac{e}{m}\frac{\partial}{\partial\vec{V}}\int\vec{k}'(\varphi_{\vec{k}\omega'}\, f_{\vec{k}-\vec{k}'} - \langle\varphi_{\vec{k}'\omega'}\, f_{\vec{k}-\vec{k}',\omega-\omega'}\rangle)\, d\vec{k}'\, d\omega$$

where ω , ω' , $\vec{k}$ and $\vec{k}'$ are the angular frequencies and wave numbers of the waves under nonlinear coupling. $\varphi_{\vec{k}\omega}$ and $f_{\vec{k}\omega}$ represent the potential and the distribution functions in Fourier transformed space and $\vec{v}$, e and m are the electron velocity, charge and mass, respectively. Due to the assumption of weak interaction, the individual dispersion relations for each of the coupled waves are obtained by neglecting the second term on the right hand side of eq.(9), i. e., the integration term. The resulting first order solution is then used with the entire eq.(9) in order to second order correction. One of the important results of this nonlinear interaction is the three wave decay process which is described by eqs.(7) and (8). An application of this concept of weak turbulence will be discussed in detail in Sec. VI.

The equation which can be obtained by neglecting the last term in eq.(9) is basically the linearized Vlasov equation from which the linear dispersion equation is obtained. This dispersion relation, which has been summarized by Stix[11] for the magneto-active warm plasma, can be derived from the wave equation

$$\vec{n}\times\vec{n}\times\vec{E} + (K)\,\vec{E} = 0 \qquad (10)$$

where $\vec{n} = (c/\omega)\,\vec{k}$, and c is the velocity of light. The matrix (K) is the equivalent dielectric tensor for the magnetoactive warm plasma with a Maxwellian velocity distribution function. The elements of the tensor (K) have the form

$$(K) = \begin{Bmatrix} K_{xx} & K_{xy} & K_{xz} \\ K_{yx} & K_{yy} & K_{yz} \\ K_{zx} & K_{zy} & K_{zz} \end{Bmatrix}$$

where (from eqs.(8) and (11) of chapter 9 of Stix[11])

$$K_{xx} = 1 + i\frac{\pi^2}{\omega\Omega}\left(\frac{-\Omega e^{-\lambda}\kappa T_\perp}{mk_z}\right)\sum_{n=-\infty}^{\infty}\frac{n^2}{\lambda} I_n \langle\Theta\rangle_n$$

$$K_{xy} = -i\frac{\pi^2}{\omega\Omega}\left(\frac{-\Omega e^{-\lambda}\kappa T_\perp}{mk_z}\right)\sum_{n=-\infty}^{\infty} in\,(I_n - I_n')\langle\Theta\rangle_n$$

$$K_{xz} = -i\frac{\pi^2}{\omega\Omega}\left(\frac{e^{-\lambda}\kappa T_\perp}{mk_z}\right)\sum_{n=-\infty}^{\infty}\frac{nk_x}{\lambda} I_n \{n\langle\Phi\rangle_n - \langle\psi\rangle_n\}$$

$$K_{yx} = i \frac{\pi^2}{\omega\Omega} \left(\frac{\Omega e^{-\lambda} \kappa T_\perp}{m k_z} \right) \sum_{n=-\infty}^{\infty} - in (I_n - I'_n) \langle \Theta \rangle_n$$

$$K_{yy} = 1 - i \frac{\pi^2}{\omega\Omega} \left(\frac{\Omega e^{-\lambda}}{m k_z} \right) \sum_{n=-\infty}^{\infty} \left(\frac{n^2}{\lambda} I_n + 2\lambda I_n - 2\lambda I'_n \right) \langle \Theta \rangle_n$$

$$K_{yz} = i \frac{\pi^2}{\omega\Omega} \left(\frac{e^{-\lambda} \kappa T_\perp}{m k_z} \right) \sum_{n=-\infty}^{\infty} - i k_x (I_n - I'_n) (n \langle \Phi \rangle_n - \langle \psi \rangle_n)$$

$$K_{zz} = 1 + i \frac{\pi^2}{\omega\Omega} \left(\frac{\Omega e^{-\lambda}}{k_z} \right) \sum_{n=-\infty}^{\infty} I_n \{ n \langle v_z \Phi \rangle_n - \langle v_z \psi \rangle_n \}$$

In the above expression ; π , Ω , $T_\perp$, m, k_x, k_y and v_z are the plasma angular frequency, the cyclotron angular frequency, the temperature corresponding to the velocity component parallel to the magnetic field, particle mass, the z and x components of the wave vector $\vec{k}$, and the z component of the particle velocity $\vec{v}$, respectively. The function I_n in eq. (11) is the modified Bessel function with argument λ ($\equiv k_x^2 \kappa T_\perp / m$) and I'_n repreaents its first derivative, $\langle \Theta \rangle_n$, $\langle \Phi \rangle_n$, $\langle \psi \rangle_n$, $\langle v_z \Phi \rangle$ and $\langle v_z \psi \rangle$ are functions with arguments $T_\parallel$, $T_\perp$, ω , Ω , k_x and k_z .[11] Where $T_\parallel$ is the temperature for the particle motion parallel to the magnetic field.

The wave equation in the source free region, i.e. eq.(10), can be rewritten as

$$\begin{bmatrix} -n_z^2 + K_{xx} & K_{xy} & n_x n_z + K_{xz} \\ K_{yx} & -n_x^2 - n_z^2 + K_{yy} & K_{yz} \\ n_x n_z + K_{zx} & K_{zy} & -n_x^2 + K_{zz} \end{bmatrix} \begin{bmatrix} E_x \\ E_y \\ E_z \end{bmatrix} = 0$$

$$\begin{bmatrix} -n_z^2 + K_{xx} & K_{xy} & n_x n_z + K_{xz} \\ K_{yx} & -n_x^2 - n_z^2 + K_{yy} & K_{yz} \\ n_x n_z + K_{zx} & K_{zy} & -n_x^2 + K_{zz} \end{bmatrix} = 0$$

IV. 2. Confirmation of Wave-Wave Resonant Interaction

The condition of three wave resonant interaction suggested by solving eq.(13) corresponding to various propagation angles θ, where $\theta = \cos^{-1}(\vec{k}\cdot\vec{B}_0 / kB_0)$ as shown in Fig.6a. The

dispersion curves for $\theta = 90^\circ$ is shown in Fig.6b; the values are close to the $\theta = 85^\circ$ curve when $0 < kR < 1.0$, where $R = \sqrt{kT/m(2\pi f_H)^2}$. In the nonlinear process where many waves are mixed under the weak turbulent condition, the frequency range is not specified. In the present case, however, the observations (see eqs. (1) and (2)) indicate that the wave associated with the frequency $2f_H$ plays a fundamental role. This role is a refrection of the $2f_H$ resonance characteristics as described by the following two points :

The first characteristic is that absorption of wave energy associated with $2f_H$-wave becomes stronger when the frequency becomes closer to $2f_H$ (see an extrapolation of curves in Fig.5). On the contraly the instability becomes more difficult to trigger when the frequency becomes closer to $2f_H$; i.e., extremely higher temperature anisotropy is required for the electrostatic electron cyclotron second harmonic wave instability (this will be discussed in Sec. V). The second characteristic is that the wave energy can be trapped due to a slow group velocity. The closer the frequency aproaches to $2f_H$, the slower is the group velocity (see the slope $|\partial\omega/\partial\vec{k}|$ of the dispersion curves in Figs.6a and 6b).

To show that the experimental results given in eqs. (1) to (4) satisfy the condition of three wave resonant interaction (three wave decay) of the electrostatic electron cyclotron harmonic waves, eqs.(7) and (8) have been solved by a graphycal technique using the dispersion curves computed using eq.(13) as

given in Figs.6a and 6b, and using the other result[14]. As indicated above, the resonant characteristics are revealed in a frequency range near to $2f_H$ but slightly below $2f_H$. For the simplicity of illustration it is represented by frequency $2f_H$. For $f_2 = 2f_H$ then, $\vec{k}_2(f_2) \simeq 0$ (see Figs.6a and 6b) ; and eqs.(7) and (8) are rewritten as

$$f_3 - f_1 = 2f_H \qquad (14)$$

$$\vec{k}_3(f_3) - \vec{k}_1(f_1) \simeq 0 \qquad (15)$$

The limitation on angle θ considering here is not unique but is selected to give minimum thermal plasma damping for stable plasma. From this stand point the angle should be close to 90°, say $85^\circ < \theta < 90^\circ$. In this case vector $\vec{k}_1$, $\vec{k}_2$ and $\vec{k}_3$ are approximately in a same line ; and it follows that

$$k_3(f_3)R = k_2(f_2)R \qquad (16)$$

Using the dispersion curves given in Fig. 6a for 85° solutions to satisfy eqs.(14) and (16) are obtained at a point A ($f_1 = 1.77f_H$, $k_1(f_1) = 0.55/R$) and a point B ($f_3 = 3.77f_H$, $k_3(f_3) = 0.55/R$), i.e., the points A and B are in a same line of $kR = 0.55$ with a gap 2 in terms of f/f_H(see Fig.6a). In the real case, the $2f_H$ wave is not restricted in the frequency $2f_H$ but covers a band width below $2f_H$. To see effect of this frequency band coverage, it is here assumed that $2f_H$ wave resonance characteristics is effective in $(f - 2f_H)/2f_H < 0.01$. In this case it follows that $|\vec{k}_2(2f_H)| \lesssim 0.1/R$. The two solutions are then $3.80 \gtrsim f_3 \gtrsim 3.76$ for $0.60/R \gtrsim k_3(f_3) \gtrsim 0.50/R$ and $1.78 \gtrsim f_1 \gtrsim 1.76$ for $0.60/R >$

$k_1(f_1) > 0.50/R$, respectively. These f_3 and f_1 are also within a band width of f_{Q3} and f_{D1}.

The solution is nearly same for the case of $\theta = 90°$ since the dispersion curves for $85°$ and $90°$ are nearly same. For this reason the condition for the three wave resonant interaction was checked by using the dispersion curves for $\theta = 90° 15'$. Calculations in the interval $2.0 < f_N/f_H < 4.5$ (in steps of 0.5) indicate that the empirical eqs.(1) and (2) satisfy the three wave decay condition given by eqs.(7) and (8). When f_{D1} is in the range $1.45f_H < f < 1.5f_H$, it shows a relatively large upward frequency shift, and when it is in the range $1.60f_H < f < 1.65f_H$, it shows a relatively large downward frequency shift with respect to the relations given by eqs.(1) and (2). These frequency shifts will also be discussed in Sec.IV relating to the electrostatic electron cyclotron harmonic wave instability. When the f_2 (with $\vec{k}_2(f_2)$) waves in eqs.(7) and (8) is replaced by f_H-wave, the f_3 and f_1 frequencies obtained by the same method as the case of $2f_H$-wave coincide with the experimental results given by eqs.(3) and (4).

The angle limitation becomes less restrictive when the electrostatic electron cyclotron harmonic wave instabilities are considered (this will be discussed in Sec.V). The relation given by eq.(7) is, here, rewritten for relatively wide angle range range of the propagation vector, as

$$k_2 = \sqrt{k_1^2 + k_3^2 - 2k_1k_3 \cos\theta_{13}} \qquad (17)$$

where θ_{13} is the angle between the vector $\vec{k}_1$ and $\vec{k}_3$. When it is again assumed that $k_2 \lesssim 0.1/R$, the allowance angle θ_{13} to satisfy eqs.(9) and (12) is $\theta_{13} \simeq \pm 0.1/k_1R$ for $(k_1 \simeq k_3)$. Since $k_1R \simeq 0.55$ (see the previous discussion for $\theta \simeq 90°$), a limit of angle deviation is approximately $\pm$ 10° from the co-linear direction. The existence of this allowance angle indicates that f_1 and f_3 band widths are expanded in a certain broader range compared with the case of narrow angle near $\theta \simeq 90°$.

Thus with a coincidence of theory and experiment, it is concluded that the f_{D1} and f_{D2} waves are produced by three wave decay processes between the $2f_H$ and f_{Q3} waves and between the $2f_H$ and f_{Q4} waves, respectively ; also, the f_{D11} and f_{D21} waves are produced by three wave decay processes between the f_H and f_{Q2} waves and between the f_H and f_{Q3} waves respectively.

V. Linear Cyclotron Harmonic Wave Instability and Time Duration of f_{Dn}

As indicated in Sec.III, a temperature anisotropy is produced by the high power sounder pulse because more energy is absorbed by the electrons in the perpendicular direction than in the parallel direction. This temperature anisotropy, which is expressed as $T_\parallel/T_\perp < 1$, leads to the electrostatic electron cyclotron harmonic wave instability which was first investigated by Harris[16] and later by Hall[17] et al and Terashima[18]. The above authors restricted their investigation to the vicinity

of the electron cyclotron harmonic frequencies. The frequency range of interest in the present discussion, however, is the entire region between the harmonic frequencies. Shima and Hall[19] indicated that the instability or marginal stablity region exists in the frequency range $n + \frac{1}{2} < f/f_H < n + (1-T_\parallel/T_\perp)$ $(n=1,2,....)$. A bi-Maxwellian velocity distribution was used for the equilibrium velocity distribution function in their analysis. In this paper, more extensive results for the instability regions and growth rates of the wave are presented in f/f_H - kR planes for various values of $T_\parallel/T_\perp$ and f_N/f_H over this frequency region. The starting point is the complete dispersion relation given by eq.(13). The electrostatic cyclotron harmonic wave instabilities will show up in the solutions of this dispersion equation as positive values for the imaginary part of the angular wave frequency $\omega = 2\pi f$ since solutions of the form $\exp\{i(\vec{k}\cdot\vec{r} - \omega t)\}$ are considered (the symbols have their usual significance).

In Fig.7, only the real parts of f/f_H are plotted as a function of kR for $f_N/f_H = 3.5$ and for the extreme temperature anisotropies of $T_\parallel/T_\perp = 10^{-3}$, and 5×10^{-4} ; sample calculations satisfying the instability condition are plotted as dots for $T_\parallel/T_\perp = 10^{-3}$ and open circle for $T_\parallel/T_\perp = 5 \times 10^{-4}$. The instability occurs very close to the second harmonic frequency and is localized in a relatively narrow frequency range which approaches $2f_H$ as the wave length increases, i. e., as kR decreases. This behavior is similar to the case of the cyclotron over-

stability associated with f_H due to pressure anisotropy[11]. The above location of the instability region associated with the $2f_H$ wave is consistent with the negative frequency shift[20] observed for the Alouette 2 resonance $f_N/f_H = 2$.

In Fig.8a and 8b, two example of the dispersion curves are indicated for $T_\parallel/T_\perp = 0.1$ and for $f_N/f_H = 2.0$ and 3.5 for various propagation angles θ . It is seen that the curve for $\theta = 60^\circ$ satisfies the instability condition in a range of kR values. This condition is satisfied for angles in a range $55^\circ \leq \theta \leq 73^\circ$ when $f_N/f_H=2.0$ and $55^\circ \leq \theta \leq 77^\circ$ when $f_N/f_H=3.5$. The domains of the instability in the f/f_H-kR plane are indicated in Figs. 9 to 11, for various values of f_N/f_H and $T_\parallel/T_\perp$.

Fig. 9 corresponds to $f_N/f_H = 3.5$ to indicate that the most favorable condition for the instability is in the range $1.5f_H < f < 1.6f_H$ with an approximate critical value of temperature anisotropy of $T_\parallel/T_\perp = 0.2$. For larger temperature anisotropies, i. e., $T_\parallel/T_\perp = 0.1$ in Fig.9, this instability region appears in the frequency range $2.5f_H < f < 2.7f_H$. Fig.10 is an elaboration of the $1 < f/f_H < 2$ region of Fig.9 in that a wider range of f_N/f_H and $T_\parallel/T_\perp$ values are considered. The results show that the frequency region of the instability domain is not sensitive to variations in f_N/f_H, but that are very sensitive to variations in $T_\parallel/T_\perp$; the frequency region of the instability domain expands and increases with increasing temperature anisotropy. For even higher temperature anisotropies, new expanded instability domains appear in a dramatic cyclic nature

between the higher harmonics as indicated in Fig.11; these domains corresponding to $T_{\parallel}/T_{\perp} = 0.05$ are clearly separated into the following frequency ranges $2.5f_H < f < 2.8f_H$, $3.5f_H < f < 3.8f_H$ and $4.5f_H < f < 4.7f_H$. The calculations were terminated at $5f_H$; new instability domains can exist, however, in higher frequency regions when $T_{\parallel}/T_{\perp} < 0.05$. For a given $T_{\parallel}/T_{\perp}$ value these domains in the higher frequency regions are smaller than the domains in the lower frequency regions as can also seen in Fig.9.

A comparison of the instability domains of Figs.9 and 10 with the f_{Dn} observation of Fig.3 indicates that the sharp peaks time duration of f_{D1} and f_{D2} coinside with the most favorable condition for the instability. This most favorable condition corresponds to the minimum temperature anisotropy required to initiate the instability. The duration times for f_{D2}, f_{D3} and f_{D4} (see also statement No.5 of Sec.II) is consistent with the higher temperature anisotropy required to maintain the instabilities for the higher sequence number n. The remarkable agreement between observation and theory indicates that the electrostatic electron cyclotron harmonic wave instability is the main cause in addition to the wave-wave interaction in order to produce the long enhanced f_{Dn} resonances.

VI. Wave-Particle Nonlinear Interaction for f_{Dn} and f_{Dn1} Generation

VI. 1. Definition

The evolution of wave-particle interaction of the turbulence plasma can be described in principle by solving eq.(9). In practice, however, the appoximation of weak turbulence is invoked in order to simplify the calculations. Sagdeev[5] considered this weak turbulent approximation and described the physical situation in terms of the following three mechanisms : first, the wave instability or damping due to the wave particle interaction ; second, the redistribution of particles as a reaction of the wave particle interaction and third, nonlinear wave-wave interaction (wave-wave resonant interaction). Actually these three mechanisms evolve simultaneously but under the weak turbulence assuption the evolution can be described by the linear approximation with a first order correction of the nonlinear terms as describe above. This evolution of turbulence is interpreted as a situation where a cyclotron resonance between the particles and waves prevails under the nonlinear wave-wave interaction which is described by the relation

$$2\pi \{mf_H - (f_3 \pm f_1)\} = (\vec{k}_3(f_3) \pm \vec{k}_1(f_1)) \cdot \vec{v} \qquad (18)$$

where $\vec{v}$ is the thermal velocity of the particle , and m is integers. Since $f_{Qn+2} - f_{Dn} = 2f_H$ and $\vec{k}_3(f_{Qn+2}) - \vec{k}_2(f_{Dn})=0$, as has been discussed in Sec.IV, f_{Dn} with f_{Qn+2} satisfies eq.(18) taking m=2, $f_3=f_{Qn+2}$, $f_1=f_{Dn}$ and - sign in eq.(18). This indicates that f_{Dn}, f_{Qn+2} and $2f_H$ wave system is subjected to the

wave-particle resonance. This is called $2f_H$ wave-particle nonlinear interaction. Replacing $f_3 = f_{Qn+1}$ and $f_1 = f_{Dn1}$ in eq.(18) the above description can also be used for the definition of the f_H wave-particle nonlinear interaction.

VI. 2. $2f_H$ Wave-particle Nonlinear Interaction for f_{Dn} Generation

As discussed in Sec.III, the transmitted high power 100μsec RF sounder pulse is sufficient to produce $T_{\parallel}/T_{\perp} < 10^{-3}$ in the ionospheric plasma. The $2f_H$ wave can start as the result of the $2f_H$ wave instability which results from this temperature anisotropy (see Fig.7). Thus, the $2f_H$ resonance wave is produced even when the exciting frequency is far removed from the $2f_H$ frequency as is observed in the mixed mode experiment of the ISIS-A satellite (see Sec.III). The plasma will maintain such a high temperature anisotropy condition for a time interval less than 1.5msec. This conclusion follows from an investigation of the receiver response to the sounder pulse in the off resonance portion of the ionogram corresponding to the instability region associated with a high temperature anisotropy, i.e., between f_{D1} and $2f_H$ for example, (see Fig.1). In all of the ionograms investigated[4], the response was always less than 1.5msec in this frequency range where the plasma becomes theoretically unstable for the temperature anisotropy $10^{-2} < T_{\parallel}/T_{\perp} < 10^{-3}$. The duration of the instability condition should be even shorter when

$T_{\parallel}/T_{\perp} < 10^{-3}$ because a high anisotropic temperature state is more difficult to maintain than a low anisotropic temperature state.

The $2f_H$ wave particle nonlinear interaction consists of three interactions as indicated in the Subsection VI. 1. The first is the electrostatic electron cyclotron harmonic wave instability. This instability is investigated by using linear approximation (see Sec.V). For the experimental check of weak turbulence the linear treatment is justified when the parameter of the velocity distribution is changed to fit each stage of the evolution in the plasma turbulence. The second is the re-distribution of the velocity distribution function. In this case $T_{\parallel}/T_{\perp}$ is the major parameter discribing the distribution function. The third is the nonlinear wave-wave interaction or three-wave decay process which is described in Sec.IV.

In Fig.12, these three interactions are illustrated for the case of the $2f_H$ wave-particle nonlinear interaction (taking n=2). The transmitted wave (called the trigger wave) initiates the nonlinear coupling process between wave 1, wave 2, and the $2f_H$ wave even when the frequency of the trigger wave does not co-inside with the frequency of any of the other three waves. In the present discussion f_{D1} and f_{Q3} will be refered to as waves 1 and 2 in one wave-wave interaction, and f_{D2} and f_{Q4} will be refered to as wave 1 and 2 in another wave-wave interaction. Since the absorption of wave energy is most efficient near $2f_H$ (see extrapolation of curves in Fig.5), the $2f_H$ wave produced

by the three wave decay process provides a source of plasma heating that maintains the temperature anisotropy. This anisotropy keeps wave 1 (and sometimes wave 2 as well) in the instability condition. The instability maintains the turbulence and provides a continuous source for wave 1 (and sometimes wave 2 as well) as long as the required temperature anisotropy is maintained, which is necessary in order to maintain the nonlinear mechanism. For a higher temperature anisotropy, such that the instability condition for wave 2 is satisfied, a similar process exists for this wave as illustrated in the top loop of Fig.12.

Due to radiation in the form of wave 1, and 2 and $2f_H$ wave, the energy supplied by the pulse is lost from this loop system in the local plasma. The temperature anisotropy will decrease with time, and eventually the instability condition will no longer be satisfied and the system becomes stable. This condition can be illustrated in Fig.12 by opening the switches.

When the f_{D1} frequency becomes close to the edge of the frequency region $1.5f_H < f < 1.6f_H$, i.e., the region most favorable for the instability, f_{D1} shows a complicated behavior. As has been mentioned in Sec.IV, the f_{D1} shows an upward frequency shift from $f_{Q3} - 2f_H$ in the range $1.45f_H < f_{D1} < 1.55f_H$ and shows a downward frequency shift in the range $1.60f_H < f_{D1} < 1.65f_H$. This evidence is also related to the dip of the empirical relationship mentioned in statement No.3 of Sec.II. Usually the frequency $f_{Q3} - 2f_H$ covers a certain band width of $\pm \Delta f$ where $\Delta f \lesssim 0.05f_H$. In so far as $1.5f_H < f_{Q3} - 2f_H$

$\pm \Delta f < 1.6f_H$, then, the loop of wave 1 (see Fig.12) works for a long time ; the enhanced emission in the range $1.5f_H < f < 1.6f_H$ is associated with the response of $f_{Q3} - 2f_H$. Thus the center frequency, or the frequency at the longest duration portion (the definition of f_{D1}) for asymetrical resonances, is virtually shifted up for the case $1.45f_H < f_{Q3} - 2f_H < 1.55f_H$ and is shifted down for the case $1.60f_H < f_{Q3} - 2f_H < 1.65f_H$.

When f_{D1} is not in the instability domain only the nonlinear process given by eqs.(1), (2), (7) and (8) contribute to generate f_{D1}. The side loop in Fig.12, shows the mechanism[8,9] corresponding to the prolonged duration of the $2f_H$ wave. Since there is no power maintainance due to the instability the side loop effect must be a simple wave-wave interaction or linear wave trapping. The observation evidence given in Figs.2 and 3 compared with the instability domain in Fig.9 and 10 shows that the f_{D1} resonance with low duration time (less than 2msec) is systematically identified even though f_{D1} is in the frequency range where no instability can take place.

VI. 3. f_H Wave-Particle Nonlinear Interaction for f_{Dn1} Generation

The f_H wave-particle nonlinear interaction relates to the weaker diffuse resonance branches f_{D11} and f_{D21}. Replacing f_{D11} and f_{D21} by wave 1, and f_{Q2} and f_{Q3} by wave 2, the interaction is illustrated in Fig.12 with n=1. The ex-

planation is similar to that of the previous section with f_H replacing $2f_H$.

A major difference between the f_{D11} and f_{D21} diffuse resonances as compared with the f_{D1} and f_{D2} diffuse resonances is that the former group exists only when the instability condition is satisfied for at least one of the waves(compare Fig.3 with Fig.9 and 10). Thus, the f_{D11} and f_{D21} resonances do not exist strictly as a result of the three wave resonant interaction i.e., the f_H wave is quickly absorbed in the medium. Additional evidence in support of this statement is provided by the mixed mode experiment of ISIS-A, (see Fig.4), where the duration of f_H is observed to be negligibly small when the frequency of the trigger wave does not coincide with the f_H resonance frequency. The $2f_H$ resonance, on the other hand, indicates a long time duration (usually longer than 4msec) even when the frequency of the trigger wave is far removed from $2f_H$. Thus the instability condition is necessary for the production of f_{D11} and f_{D21} resonances. Since a high temperature anisotropy is required to maintain the instabilities at these frequencies (see Figs. 9, 10 and 11) the f_H wave must be more efficiently to heat the plasma than the $2f_H$ wave in order to maintain the required plasma instability.

VII. Discussion of f_{D3}, f_{D4} and the other Weaker Resonances

The physical meaning of the occurence of the f_{Dn} resonance for f_{D1}, f_{D2}, f_{D11} and f_{D21} are investigated in the previous

section in terms of $2f_H$ and f_H wave-particle nonlinear interaction. Noticing the sequential nature of f_{Dn} resonance, and three wave resonant interaction in n=1 and 2, f_{D3} and f_{D4} can also be understood to be generated by the same $2f_H$-combination mechanism even if the response of the pulse transmission corresponding to f_{Q5} and f_{Q6} can not be detected at the present experiments. As mentioned in the last part of statement No.2 in Sec.II, the weaker second resonance f_{D31} and f_{D41} statistically merges into the main branch resonance f_{D3} and f_{D4}. From the general tendency described above, however, these branches f_{D31} and f_{D41} should be produced by f_H wave-particle nonlinear interaction.

The only exception is the f_{D12} resonance (see statement No.2 in Sec. II). This resonance covers the frequency range $1.5f_H < f_{D12} < 1.6f_H$ which is most prefarable condition for the instability. No apparent correlation is seen between the f_N/f_H value and the f_{D12} frequency. The time duration of f_{D12} is usually shorter than 1.5msec. The feature of this response shows a faint cloud like shape. This evidence suggest that the electrostatic electron cyclotron harmonic wave instability can exist for non resonant wave particle interactions due to the strong power transmission itself without requiring $2f_H$ or f_H wave-particle nonlinear interaction. This frequency coincide with the most preferable portion for instability as indicated by the numerical calculation (see Figs.2 and 9).

VIII. Conclusion

The center frequency of the sequence of diffuse plasma resonances f_{Dn} is observed to be related to the electrostatic wave resonance frequency f_{Qn} and $2f_H$ in the following manner : $f_{D1}=f_{Q3}-2f_H$ and $f_{D2}=f_{Q4}-2f_H$. Also, the frequency of the weaker diffuse resonance branch f_{Dn1} (observed on the high frequency side of f_{Dn1}) is related to f_{Qn} and f_H by $f_{D11}=f_{Q2}-f_H$ and $f_{D21}=f_{Q3}-f_H$. For higher sequence numbers, the relation is not directly confirmed but the observed sequece nature suggests that the rule should be extended to $f_{Q\,n+2}=f_{Dn}+2f_H$, and $f_{Q\,n+1}=f_{Dn1}+f_H$. In addition to this frequency combination, the center frequency of f_{Dn} or f_{Dn1} definitely depends on the plasma parameter f_N/f_H. This plasma parameter dependency is explained by the three wave resonant interaction (or the tree wave decay process) of the electrostatic electron cyclotron harmonic waves where it has been shown that

$$f_{Q\,n+2}=f_{Dn}+2f_H \quad \text{with} \quad \vec{k}(f_{Q\,n+2})=\vec{k}(f_{Dn})+\vec{k}(2f_H),$$

$$\text{and} \quad f_{Q\,n+1}=f_{Dn1}+f_H \quad \text{with} \quad \vec{k}(f_{Q\,n+1})=\vec{k}(f_{Dn1})+\vec{k}(f_H).$$

Calculations based on the complete dispersion relation from linear approximation indicate that the most likely point for electrostatic electron cyclotron harmonic wave instability occurs in a frequency range $1.5f_H<f<1.6f_H$ for a temperature anisotropy $T_\parallel/T_\perp \simeq 0.2$. This region expands towards the higher frequency side (approaching $2f_H$) when the temperature anisotropy increases ($T_\parallel/T_\perp$ value becomes small). The next likely point for instability is in the frequency range $2.6f_H<f<2.7f_H$ (for $T_\parallel/T_\perp=0.1$), and regions of instability sequentially appear between the higher harmonics as the temperature

anisotropy increases.

The intense power transmission of the Alouette 2 sounder pulse produces a high temperature anisotropy and causes the electrostatic electron cyclotron harmonic wave instability. The observations indicate that this initial instability persists for no longer than 1.5msec. The observations also indicate that the longest duration time of the f_{Dn} response occurs when f_{Dn} coincides with the most favorable portion for instability. This long duration is attributed to a combined process of instability and nonlinear wave-wave interaction of the electrostatic electron cyclotron harmonic waves. The intense sounder pulse forms electric fields which are sufficient to produce a weakly turbulent plasma. After stired by the sounder pulse, the turbulence evolves including two kinds of wave-particle nonlinear interaction. One interaction involves the waves associated with the main branch of f_{Dn} and $f_{Q\ n+2}$ waves which produce the $2f_H$ wave by wave-wave nonlinear interaction. This $2f_H$ wave is effectively absorbed by the plasma to increase the perpendicular energy more than the parallel energy through the wave particle interaction; as the result of this differential heating the instability is maintained. The instability maintain the turbulence which produces f_{Dn}, $2f_H$ and $f_{Q\ n+2}$ waves. This process is called $2f_H$ wave-particle nonlinear interaction. This interaction satisfies the condition of the wave-particle interaction associated with the second harmonic cyclotron resonance as $2\pi \left\{ 2f_H-(f_{Q\ n+2}-f_{Dn})\right\} =\left\{\vec{k}(f_{Q\ n+2})-\vec{k}(f_{Dn})\right\}\cdot\vec{v}$.

The other interaction involves the waves associated with the weaker branch f_{Dn1} and $f_{Q\ n+1}$ resonances by forming f_H wave-particle nonlinear interaction as the case of $2f_H$ wave-particle nonlinear interaction. In this case, the condition $2\pi\left\{f_H-(f_{Q\ n+1}-f_{Dn1})\right\}=\left\{\vec{k}(f_{Q\ n+1})-\vec{k}(f_{Dn1})\right\}\cdot\vec{v}$ is satisfied.

The present result gives the clear interpretation on the generation mechanism of f_{Dn} and f_{Dn1} resonances. The result also indicates that the experimental prove has been given to the theory on the wave particle nonlinear interaction.

Acknowledgement

The author wishes to express his sicere thanks to Dr. R.F. Benson for his critical comment and encouragement that led to achieve the work and for his great effort devoted to proof reading of the paper. The author is grateful to Drs. R. E. Hartle and S.J. Bauer for their valuable discussion and encouragement through out this work ; and wishes to thank Mr. J. E. Jackson who suggested to summarize all the identified plasma resonance in one diagram.

References

1. W. Calvert and J. R. McAfee, Proc. IEEE, 57, 1089 (1969).

2. G. L. Nelms, R. E. Barrington, J. S. Belrose, T. R. Nartz, I. B. McDiomid, and L. H. Brace, Can. J. Phys., 44, 1419 (1966).

3. G. L. Nelms and G. E. K. Lockwood, Space Res., 7, 604 (1966).

4. H. Oya, J. Geophys. Res., 75, 4279 (1970).

5. R. Z. Sagdeev and A. A. Galeev, Nonlinear plasma theory (Edited by T. M. O'Neil), New York, Benjamin, Inc., (1969) Page 106.

6. G. E. K. Lockwood, Can. J. Phys., 41, 190 (1963).

7. E. S. Warren and E. L. Hagg, Nature, 220, 466 (1968).

8. F. A. Fejer and W. Calvert, J. Geophys. Res., 69, 5049 (1964)

9. F. W. Crawford, R. S. Harp, and T. D. Mantei, J. Geophys. Res., 72, 57 (1967).

10. C. A. Franklin and M. A. Maclean, Proc. IEEE, 57, 897 (1969).

11. T. H. Stix, The theory of plasma waves, New York: McGraw-Hill (1962).

12. B. B. Kadomtsev, Plasma turbulence, Academic Press, New York (Edited by M. G. Rusbridge) 1965 (page 31-35).

13. A. Sjölund and L. Stenflo, Nonlinear coupling in a magnetized plasma, Z. Phys., 204, 211 (1967).

14. H. Oya, NASA Goddard document, X-621-70-352 and submitted to Radio Science (1971).

15. C. F. Kennel and F. Engelmann, Phys. Fluids, 9, 2377 (1966).

16. E. G. Harris, Phys. Rev. Lett. 2, 34 (1959).

17. L. S. Hall, W. Heckrotte, and T. Kammash, Phys. Rev. 139, A1117 (1965).

18. Y. Terashima, Progress Theo. Physics, 37, 661 (1967).

19. Y. Shima and L. S. Hall, Phys. Rev. 139, A1115 (1965).

20. R. F. Genson, to be submitted to Radio Science (1971).

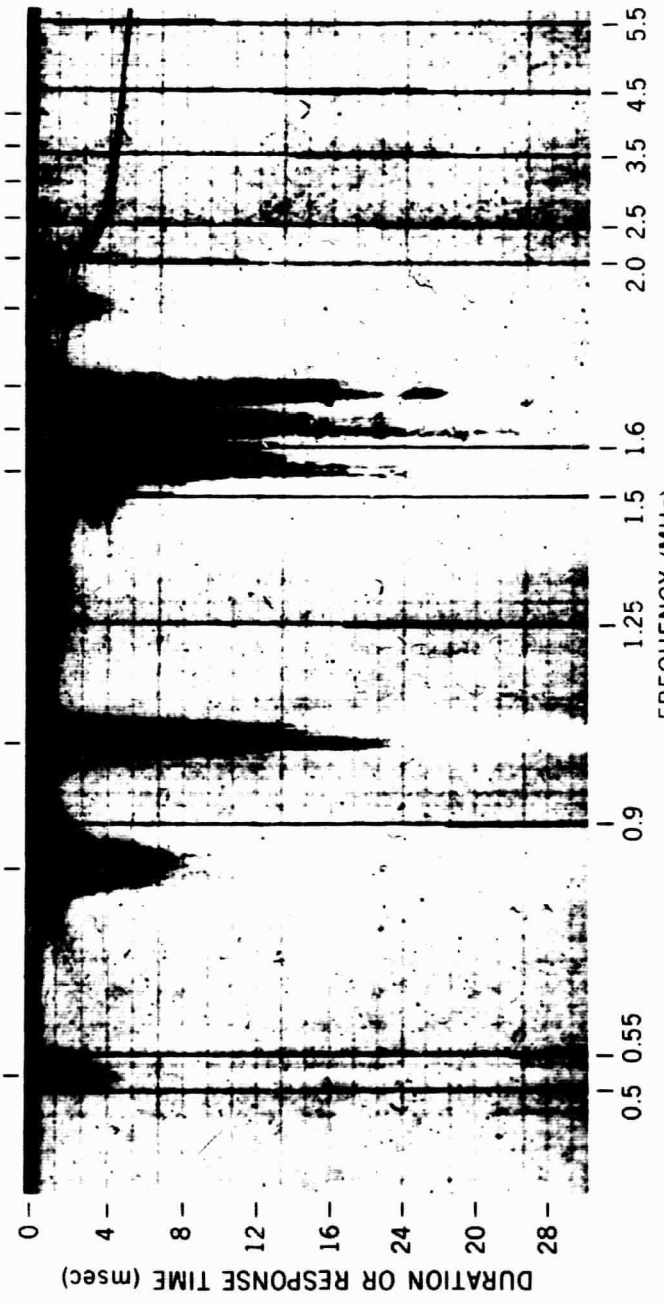

Figure 1. A sample ionogram observed by the Alouette 2 satellite at April 22, 1966, 2205:46 UT; telemetered at Santiago Station; plasma resonances are observed as prolonged responses at the cyclotron harmonic frequencies nf_H ($n = 1,2,\ldots$), respectively; f_{D1} is the first member of the sequence of diffuse plasma resonances f_{Dn}; and f_{Q3} is the third member of the so-called electrostatic wave resonance sequence the curves in the frequency range from 1.7 to 5.5MHz and a response time range from 1.3 to 4.5msec are echos from the top-side ionosphere which is located below the satellite level.

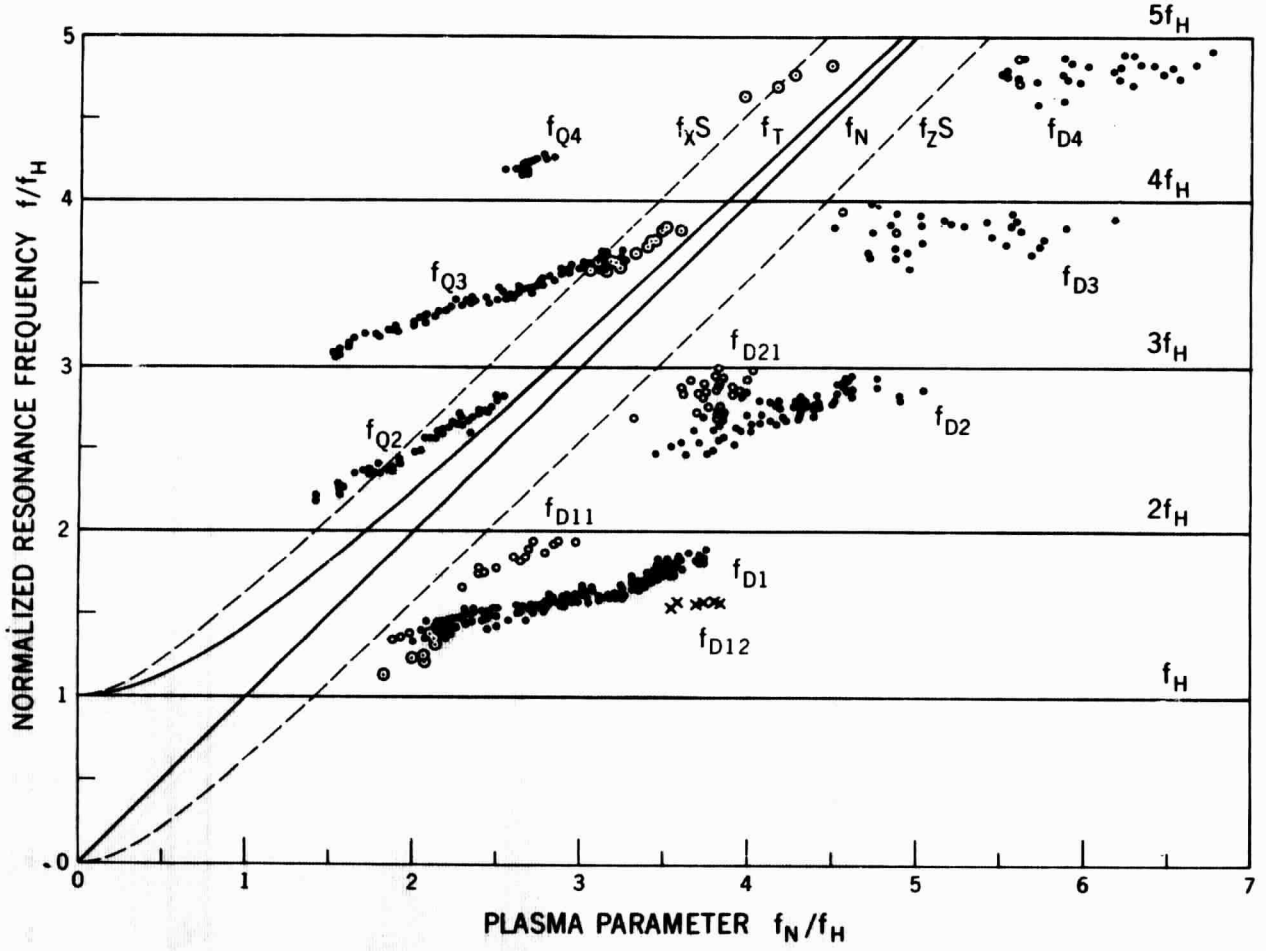

Figure 4. $f/f_H - f_N/f_H$ diagram of the resonances f_{Dn}, f_{Dn1}, f_{D12}, f_{Qn}, f_N, f_T, and n_{fH}; the cut-off frequencies at the satellite of the x and z propagations are plotted as f_xS and f_zS, respectively; or the f_{Dn} resonances, dots indicate the main branch, and open circles and x's indicate the weaker secondary branches at f_{Dn1} and f_{Dn2}, respectively; the open circles with small dots show new data which are added to the originally published data of f_{Dn} and f_{Qn}.

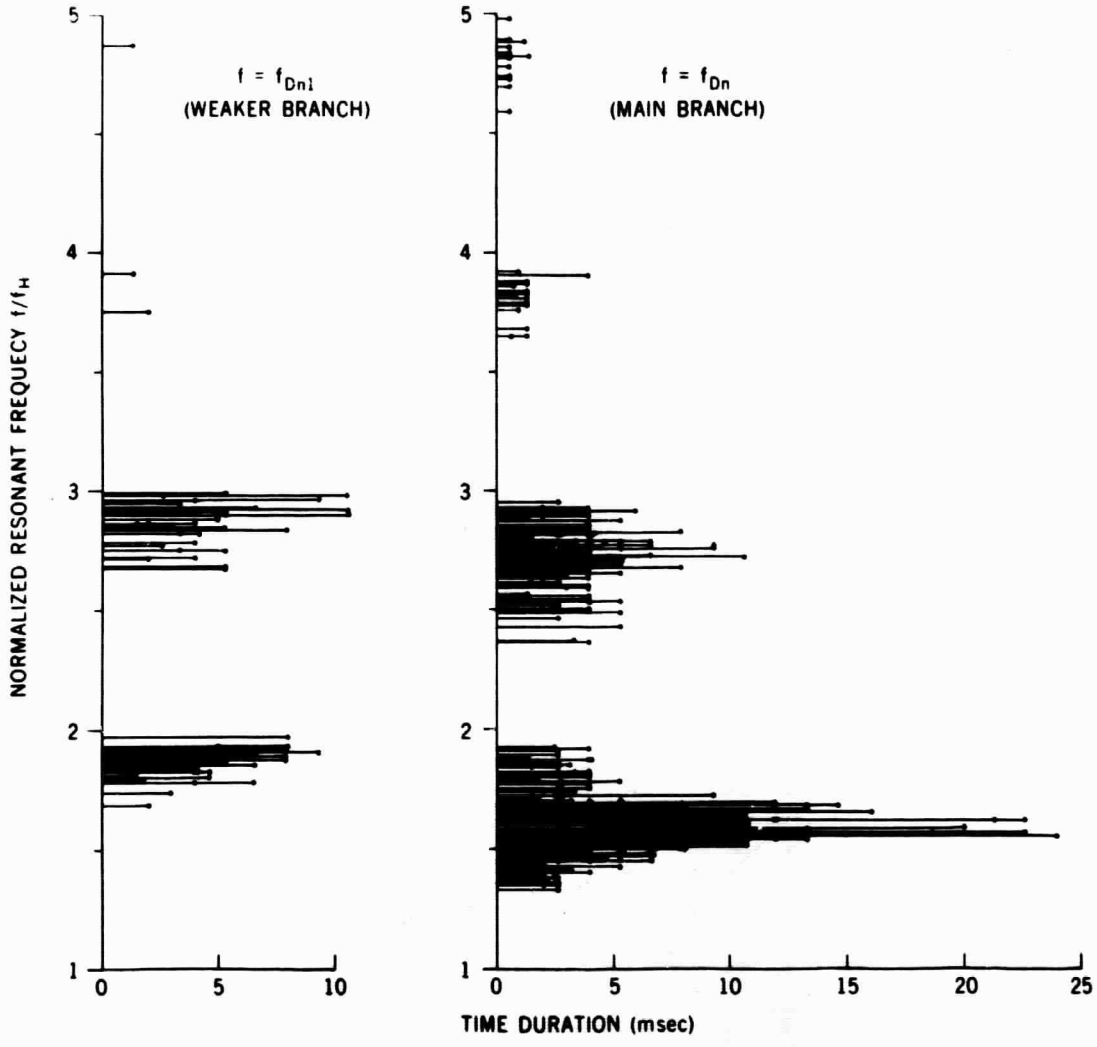

Figure 3. Time duration of f_{Dn} (dots in the top) and f_{Dn1} (open circle in the bottom) vs the f_{Dn} resonance frequency. The time duration refers to the center portion (or maximum duration portion for asymetrical cases) of the resonance.

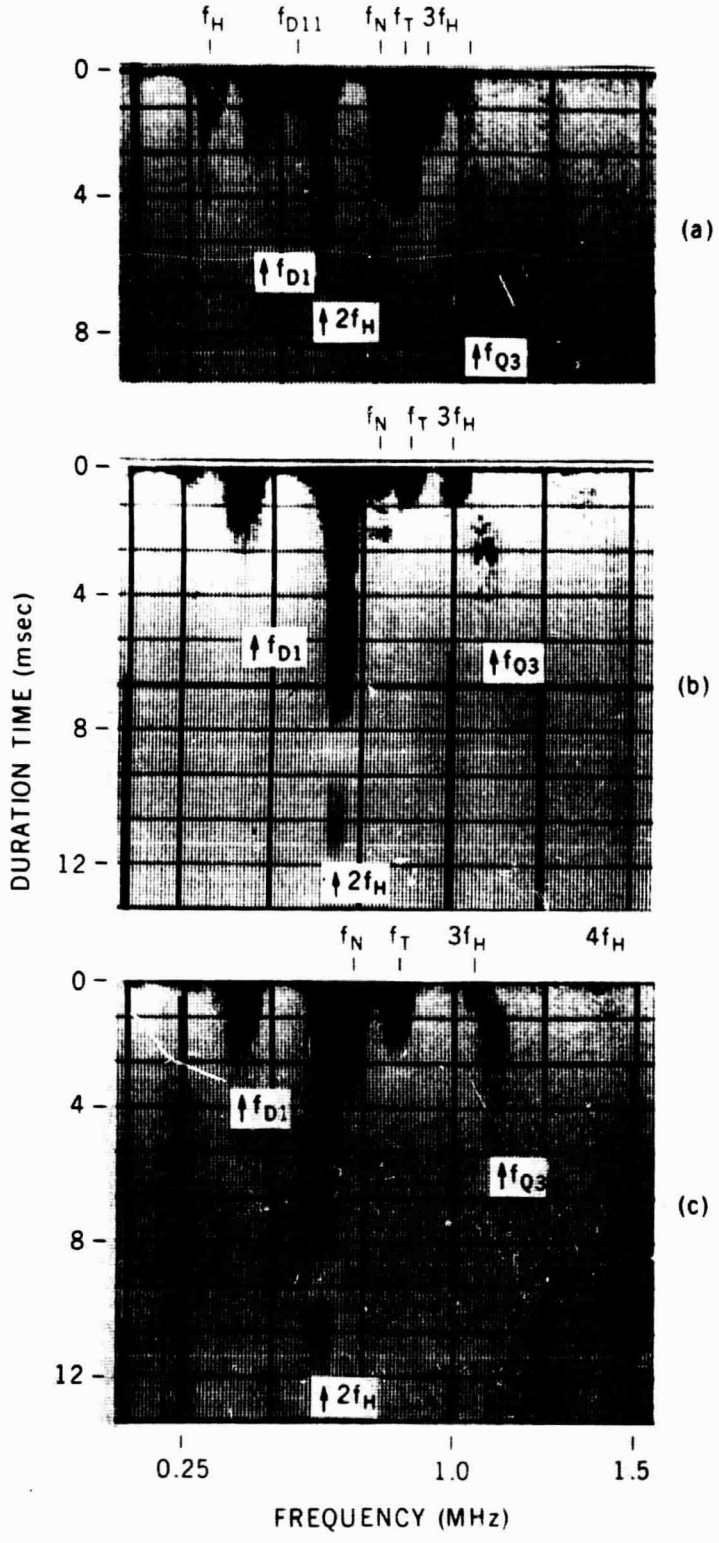

Figure 4. A series of ISIS-A mixed mode ionogram obtained over the Ottawa telemetry station in April 23, 1969; at a) 2230:35 UT altitude 3420 km, b) 2227:52 UT; 3355 km and c) 2226:31 UT; 3345 km.

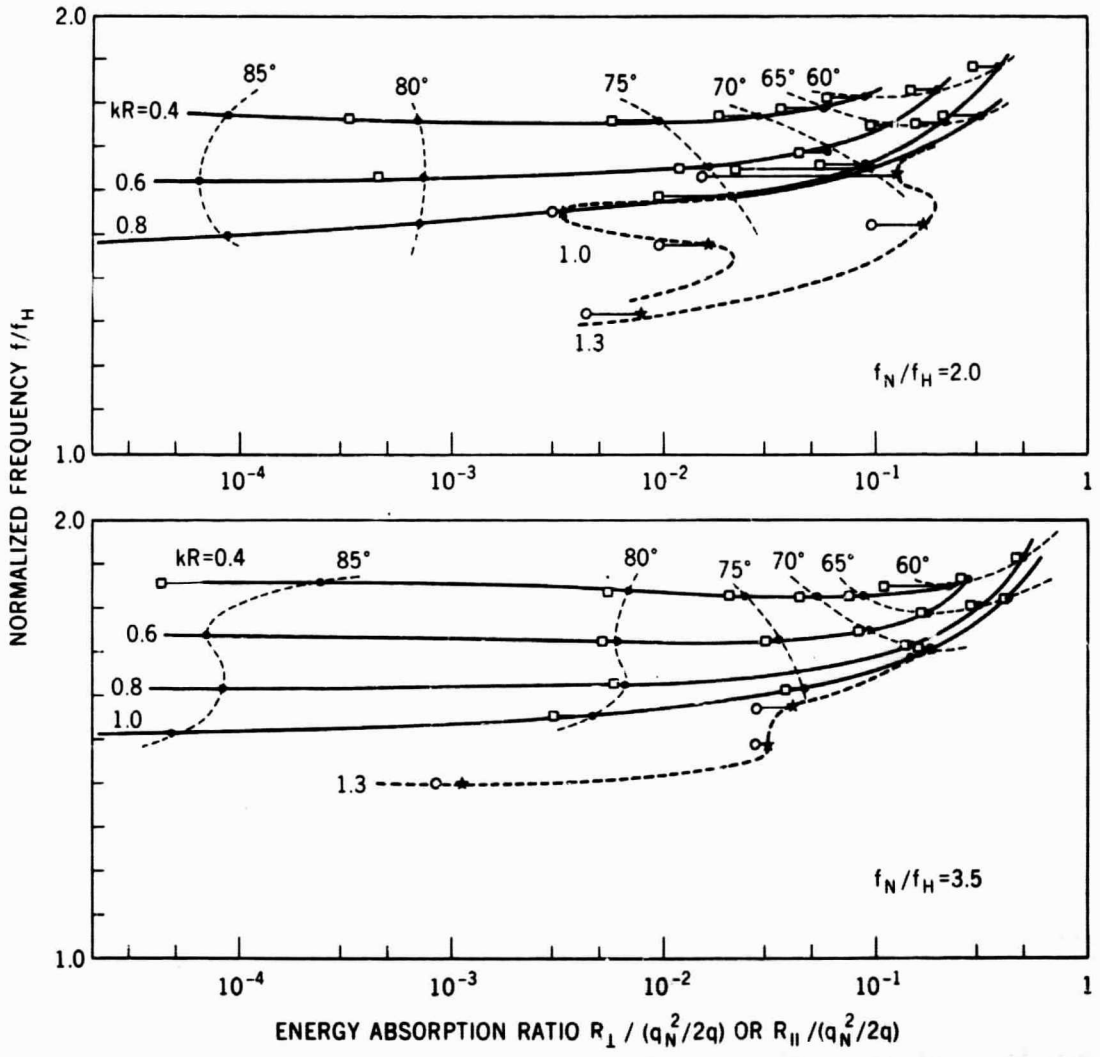

Figure 5. Energy absorption ratio $R_{||}$ and $R_{\perp}$ versus frequency for $f_N/f_H = 2.0$ and 3.5; the ratios are normalized by $q_N^2/2q$; symbols used in the diagrams are: dots for $R_{\perp} > 0$, stars for $R_{\perp} < 0$, open squares for $R_{||} < 0$ and open circles for $R_{||} > 0$; $R_{\perp}$ and $R_{||}$ are expressed as a pair for a given kR and the propagation angles given in degree.

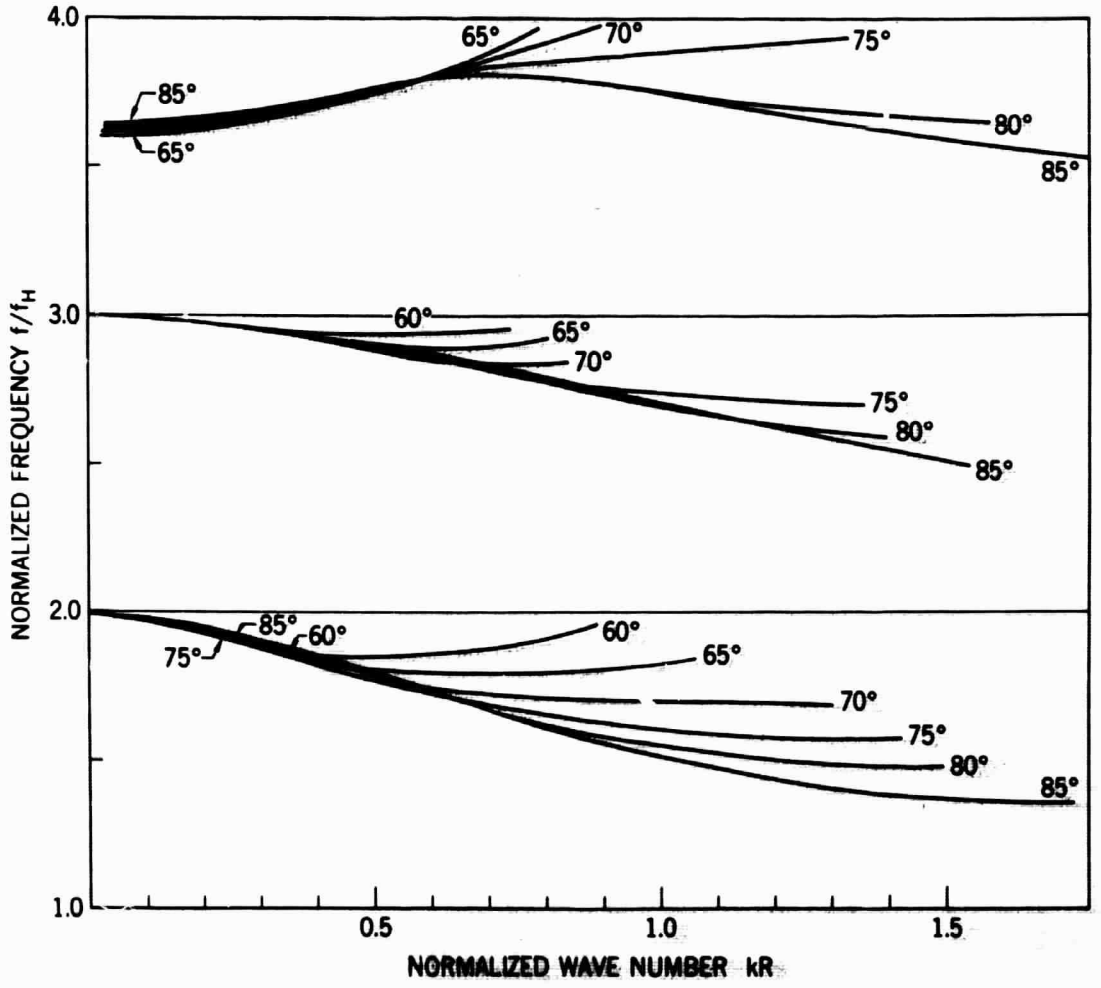

Figure 6a. Dispersion curves of the electrostatic electron cyclotron harmonic waves for $T_{\parallel}/T_{\perp} = 1$, $f_N/f_H = 3.5$, and various propagation angles θ; only the real part of the frequency is plotted (curves corresponding to high negative value of the imaginary part of the frequency are not presented).

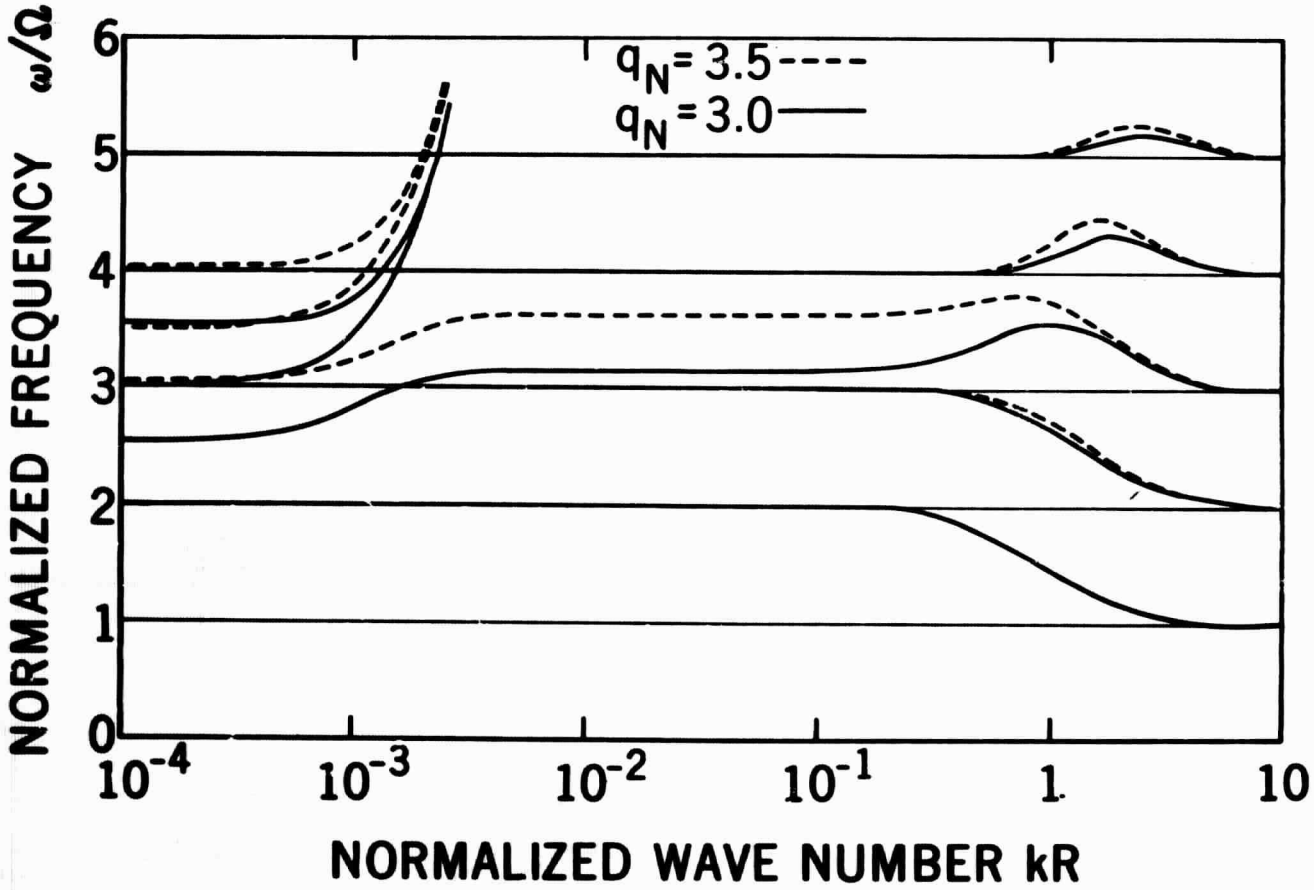

Figure 6b. The dispersion curves of the electrostatic electron cyclotron harmonic waves for the propagation angle $\theta = 90°$ obtained for all wavelengths.

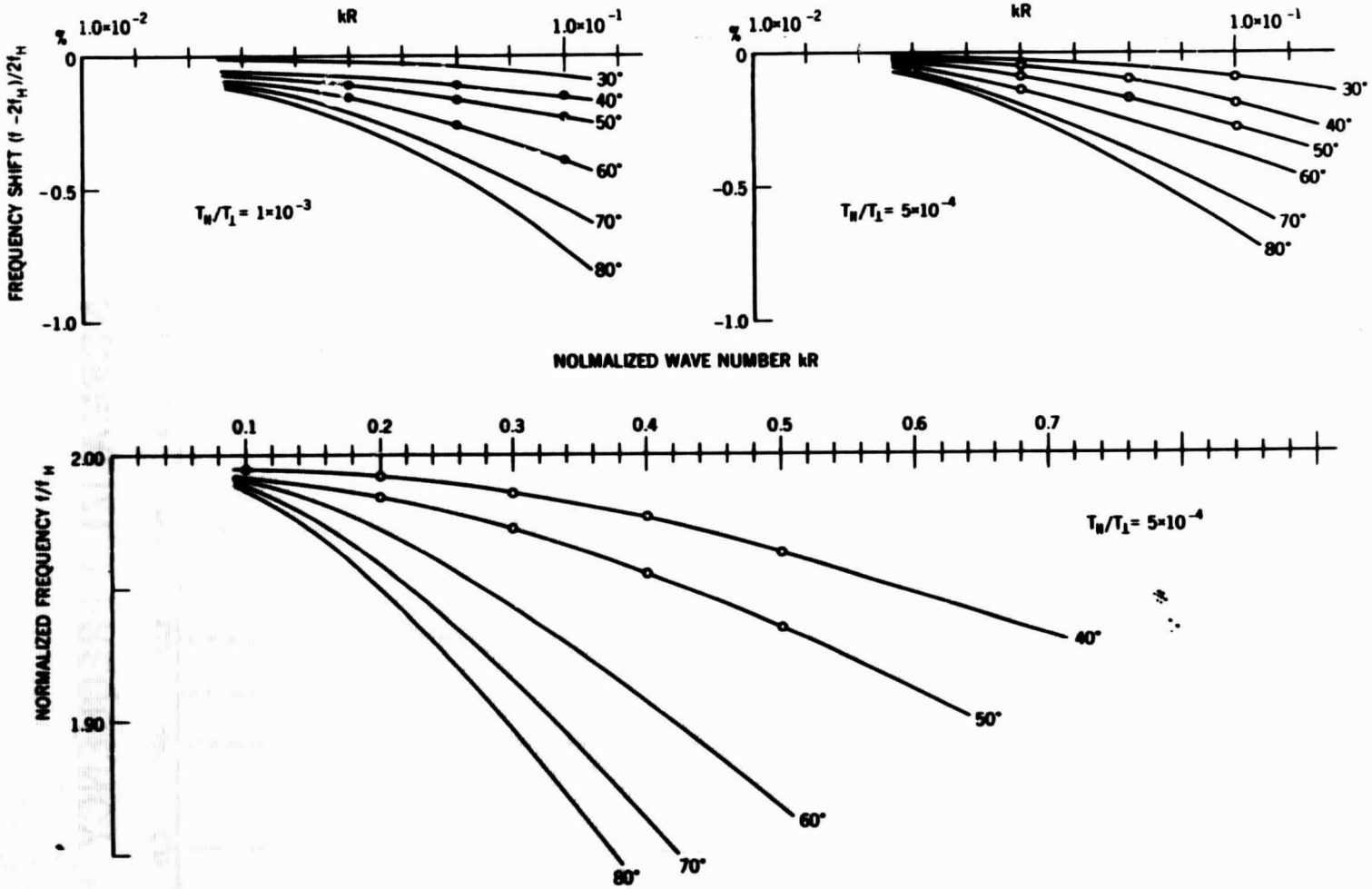

Figure 7. The dispersion curves near $2f_H$ for $f_N/f_H = 3.5$ real parts of the frequency f and for temperature anisotropies of $T_{II}/T_{\perp} = 5 \times 10^{-4}$ and 10^{-3}; the sample points where the imaginary part of f become positive are plotted by dots for $T_{II}/T_{\perp} = 10^{-3}$ and open circles for $T_{II}/T_{\perp} = 5 \times 10^{-4}$.

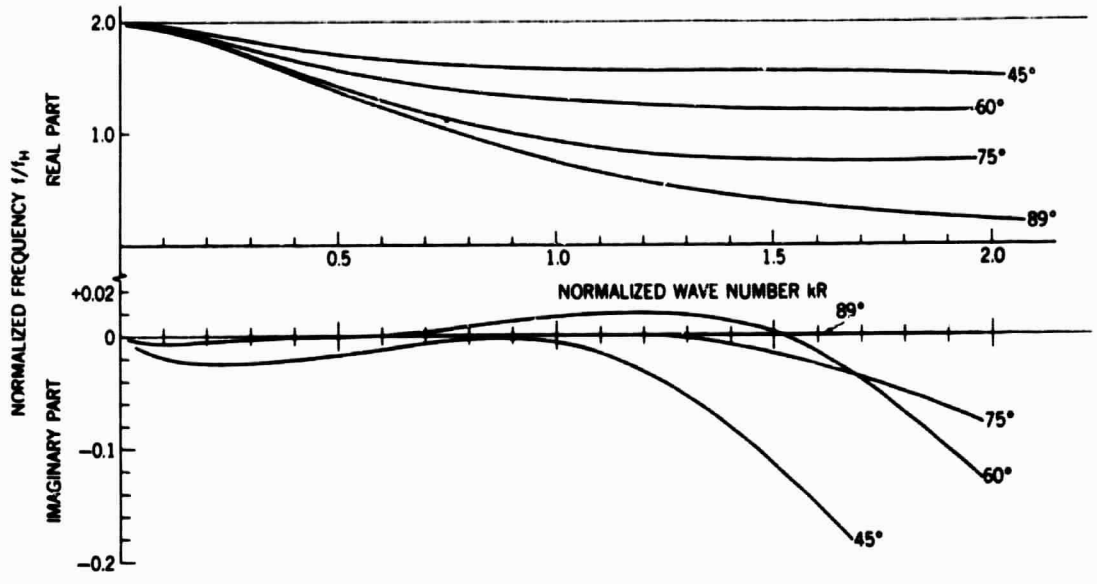

Figure 8a. Dispersion curves of the electrostatic electron cyclotron harmonic waves for $T_{\parallel}/T_{\perp}$ = 0.1 and f_N/f_H = 2.0; the normalized real and imaginary parts of the frequency are plotted versus kR; a positive portion of the imaginary part corresponds to the electrostatic electron cyclotron harmonic wave instability.

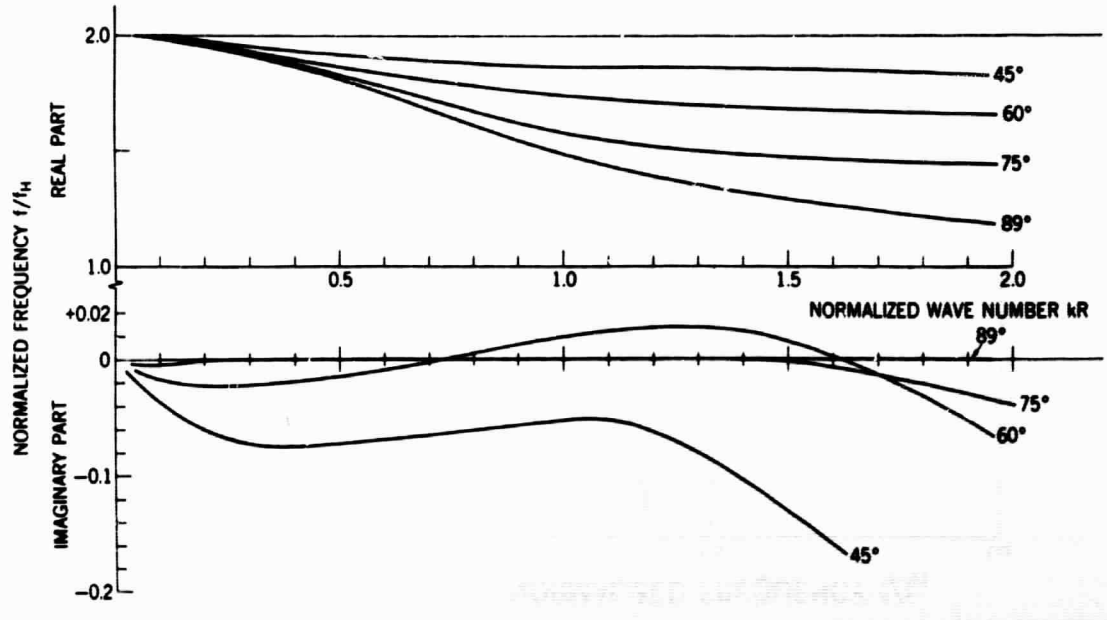

Figure 8b. Dispersion curves of the electrostatic electron cyclotron harmonic waves for $T_{\parallel}/T_{\perp}$ = 0.1 and f_N/f_H = 3.5; the normalized real and imaginary parts of the frequency are plotted versus kR; a positive portion of the imaginary part corresponds to the electrostatic electron cyclotron harmonic wave instability.

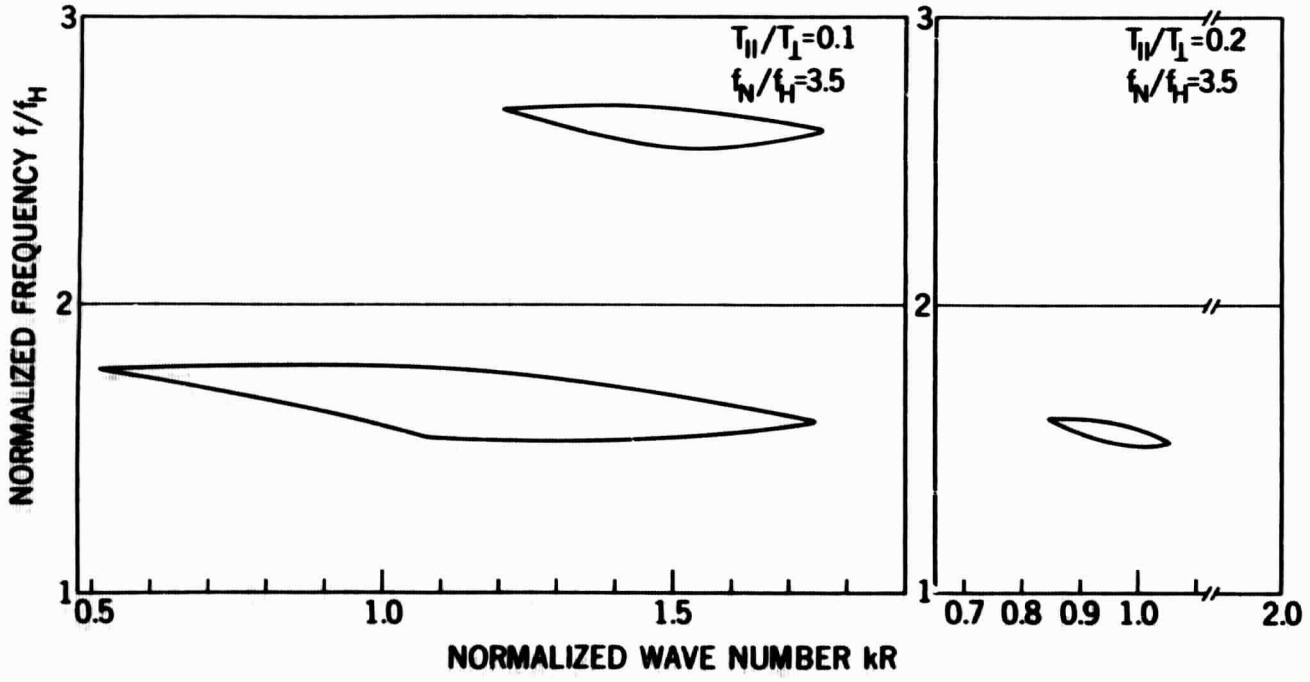

Figure 9. Instability domains in f/f_H – kR plane (inside the closed loops) for $T_{II}/T_{\perp} = 0.2$ and 0.1, both for $f_N/f_H = 3.5$.

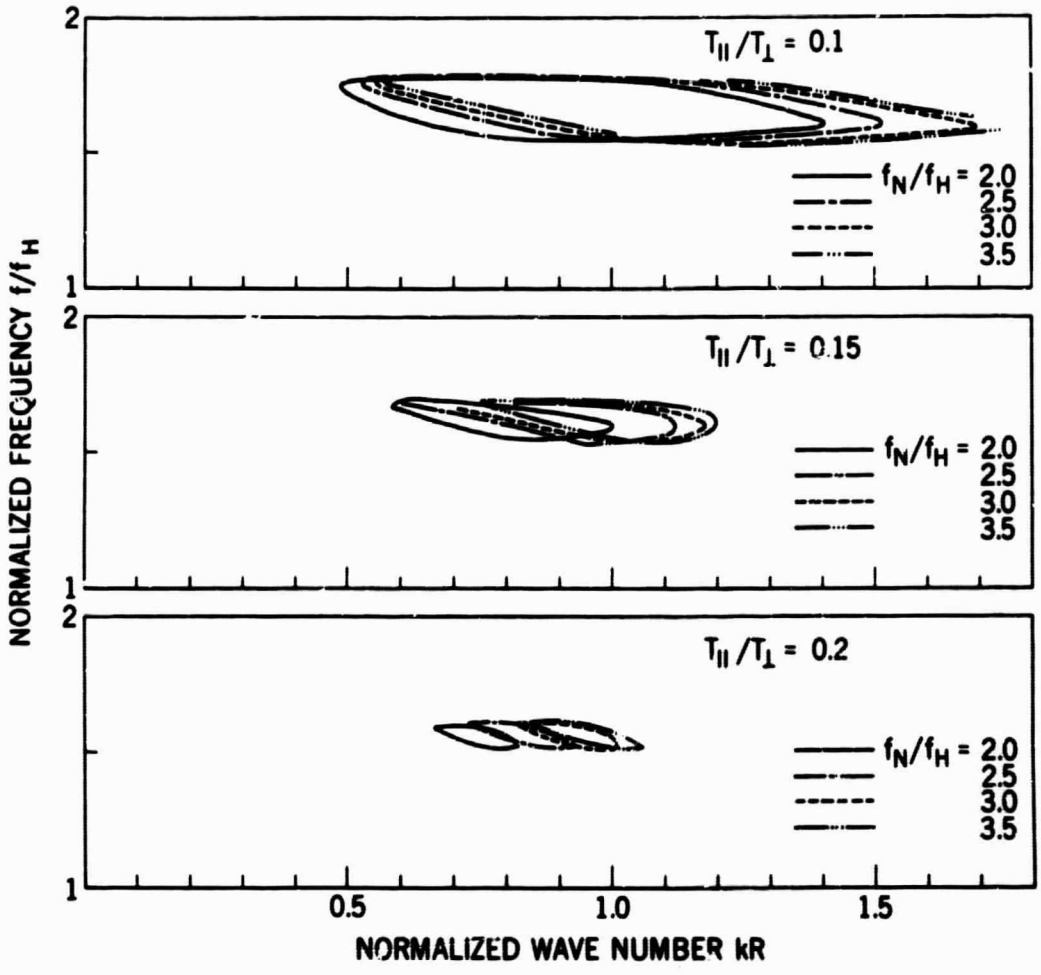

Figure 10. Instability domains in f/f_H – kR plane (inside the closed or half closed loops) for $T_{II}/T_{\perp}$ = 0.2, 0.15, and 0.1; and f_N/f_H = 2.0, 2.5, 3.0 and 3.5 for indicated curves, respectively.

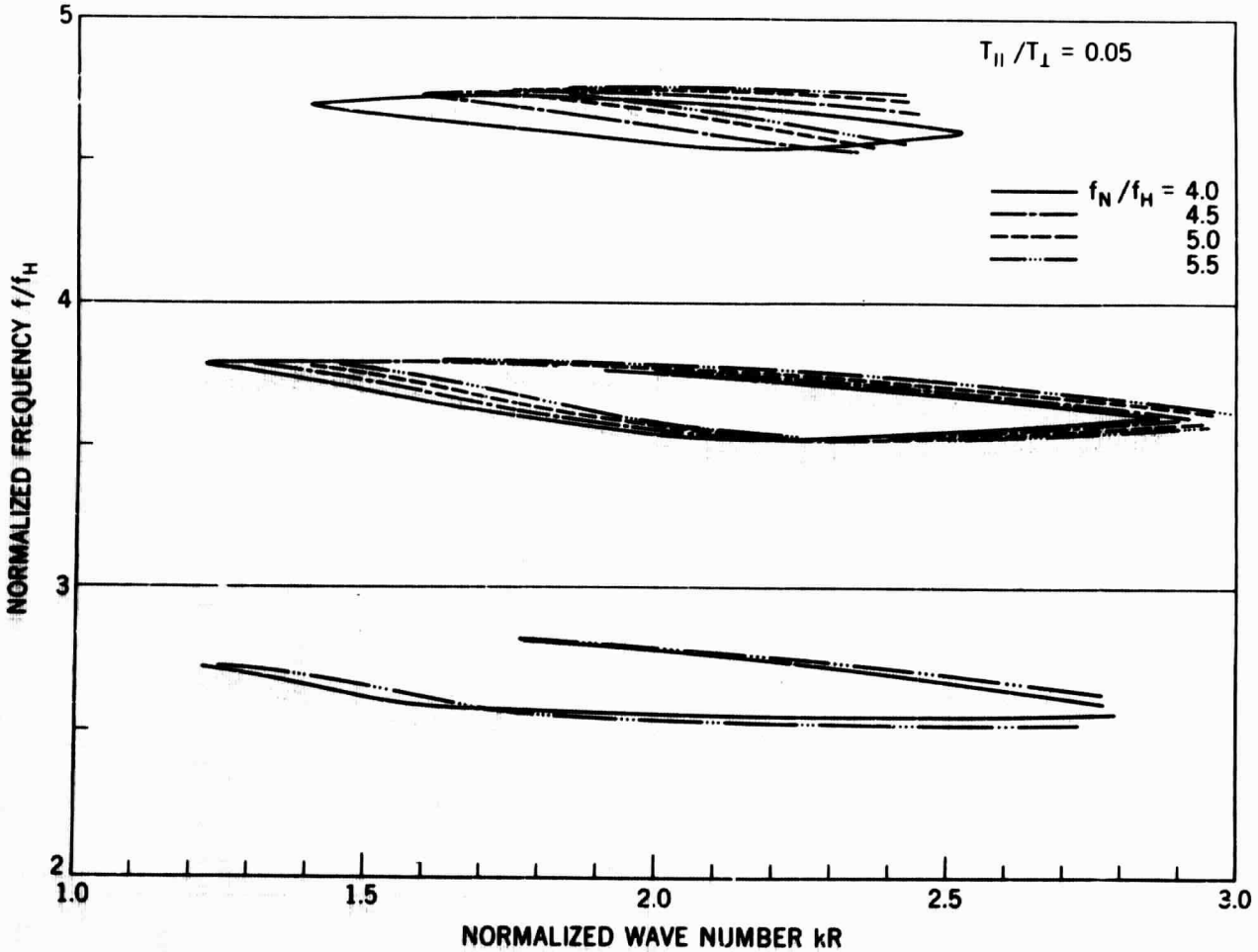

Figure 11. Instability domains in $f/f_H - kR$ plane (inside the closed or half closed loops) for $T_{II}/T_{\perp} = 0.05$ and $f_N/f_H = 4.0, 4.5, 5.0$ and 5.5 for indicated curves; the curves for $f_N/f_H = 4.5$ and 5.0 are taken out in the frequency range $2 < f/f_H < 3$, because no significant change is revealed.

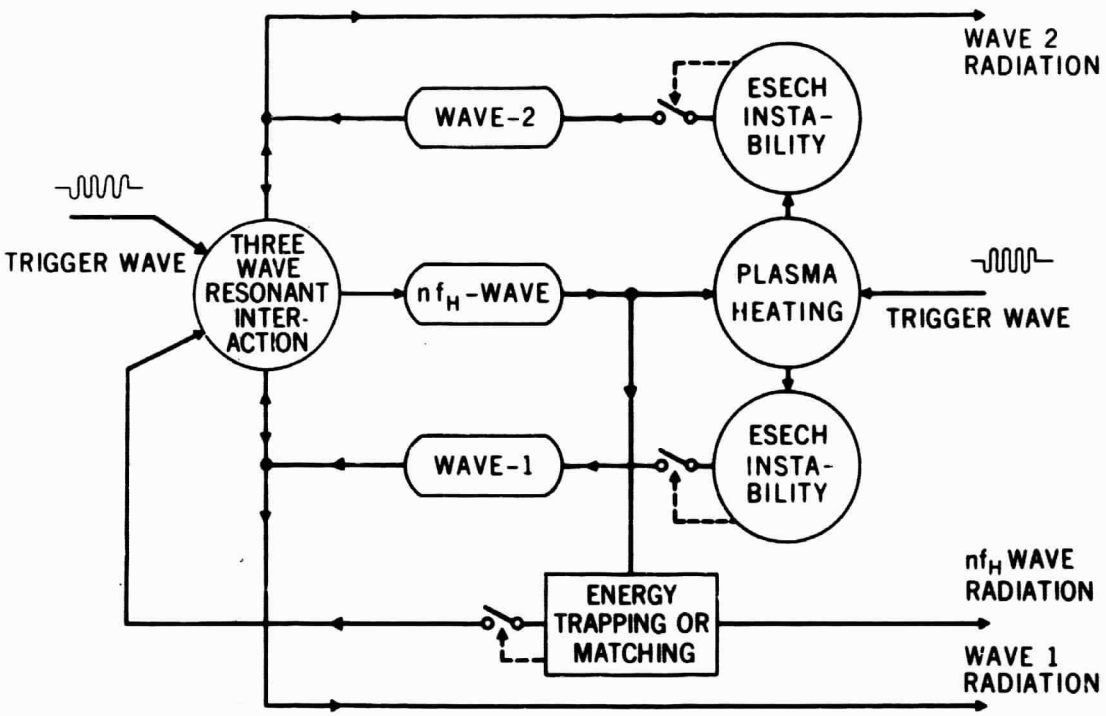

Figure 12. Block diagram to show the nf_H wave-particle nonlinear interaction; ESECH is an abbreviation for electron cyclotron harmonic waves; n = 1 or 2 corresponding to each case.